

## CHAPTER 44

### FORMULATION AND VALIDATION OF VERTICALLY 2-D SHALLOW-WATER WAVE MODEL

Bradley D. Johnson<sup>1</sup>, Nobuhisa Kobayashi<sup>2</sup>, and Daniel T. Cox<sup>3</sup>

#### Abstract

A numerical model is developed to predict the time-dependent, two-dimensional velocity field under normally incident breaking waves on beaches and coastal structures. Use is made of the depth-integrated continuity and horizontal momentum equations, where the momentum equation includes the momentum flux correction due to the vertical variation of the horizontal velocity. The third equation for the momentum flux correction is derived from the depth-integrated wave energy equation together with a cubic horizontal velocity profile. The three equations are solved using the MacCormack finite difference method. The quasi two-dimensional model is compared with two laboratory data sets and is found to predict the vertical variation of the horizontal velocity measured below the trough reasonably well. However, the energy dissipation in the model is primarily numerical for breaking waves on gentle slopes despite the explicitly modeled energy dissipation due to wave breaking.

#### Introduction

The quantitative prediction of detailed sediment transport on beaches and armor stability on coastal structures requires a numerical model that can predict the time-dependent, vertically two-dimensional velocity field of breaking waves on slopes with sufficient accuracy and reasonable computation time.

Available time-dependent, one-dimensional and other numerical models for breaking and nonbreaking waves on inclined structures and beaches (e.g., Kobayashi and Wurjanto 1989) are relatively simple and robust. Generally, these models predict the free surface elevation fairly accurately, within about 20% errors. The comparisons of a one-dimensional model with the experiment for regular waves spilling on a rough, impermeable 1:35 slope conducted by Cox *et al.* (1995) indicated that the horizontal velocity measured below the wave trough level was represented by the computed depth-averaged velocity reasonably well. The temporal variation of the bottom shear stress was predicted poorly because errors in the computed horizontal velocity were magnified in the computed bottom shear stress and because the bottom friction factor was not really constant. These limited comparisons suggest that a vertically

---

<sup>1</sup>Ph.D. Student, Center for Applied Coastal Research, University of Delaware, Newark, DE 19716.

<sup>2</sup>Professor and Associate Director, Center for Applied Coastal Research, University of Delaware, Newark, DE 19716.

<sup>3</sup>Assistant Professor, Department of Civil Engineering, Texas A&M University, College Station, TX 77843-3136.

two-dimensional model will be required to predict the detailed vertical variations of the fluid velocities and shear stress which are essential for predicting cross-shore sediment transport on beaches and hydrodynamic forces acting on armor units on coastal structures.

A simplified two-dimensional model called VBREAK has been developed assuming a cubic horizontal velocity profile outside of the wave boundary layer. The vertically two-dimensional problem is then reduced to a depth-integrated one-dimensional problem in which three time-dependent, one-dimensional differential equations can be solved numerically for the water depth  $h$ , depth-averaged horizontal velocity  $U$ , and near-bottom horizontal velocity  $u_b$ . The simplified two-dimensional model is computationally as efficient as the previous one-dimensional models. As a result, the new model can be applied easily and routinely using workstations. This paper summarizes the numerical model VBREAK described in detail by Kobayashi and Johnson (1995) and the comparisons of the model to available data presented in Johnson *et al.* (1996).

### Mathematical Formulation

The approximate governing equations adopted in the numerical model named VBREAK are derived from the two-dimensional continuity and Reynolds equations

$$\frac{\partial u'_j}{\partial x'_j} = 0 \quad (1)$$

$$\frac{\partial u'_i}{\partial t'} + u'_j \frac{\partial u'_i}{\partial x'_j} = -\frac{1}{\rho} \frac{\partial p'}{\partial x'_i} - g\delta_{i2} + \frac{1}{\rho} \frac{\partial \tau'_{ij}}{\partial x'_j} \quad (2)$$

in which the prime indicates the physical variables and the summation convention is used with respect to repeated indexes. The symbols used in (1) and (2) are depicted in Fig. 1 where  $t'$  = time;  $x'_1$  = horizontal coordinate taken to be positive landward;  $x'_2$  = vertical coordinate taken to be positive upward with  $x'_2 = 0$  at the still water level (SWL);  $u'_1$  = horizontal velocity;  $u'_2$  = vertical velocity;  $\rho$  = fluid density which is assumed constant;  $p'$  = pressure;  $g$  = gravitational acceleration;  $\delta_{i2}$  = Kronecker delta; and  $\tau'_{ij}$  = sum of turbulent and viscous stresses. Assuming that the viscous stresses are negligible,  $\tau'_{ij}$  may be expressed as (e.g., Rodi 1980)

$$\tau'_{ij} = \rho \left[ \nu'_t \left( \frac{\partial u'_i}{\partial x'_j} + \frac{\partial u'_j}{\partial x'_i} \right) - \frac{2}{3} k' \delta_{ij} \right] \quad (3)$$

in which  $\nu'_t$  = turbulent eddy viscosity; and  $k'$  = turbulent kinetic energy per unit mass.

To simplify (1) and (2) with (3) in shallow water, the dimensional variables may be normalized as

$$t = \frac{t'}{T'} ; \quad x_1 = \frac{x'_1}{T' \sqrt{gH'}} ; \quad x_2 = \frac{x'_2}{H'} ; \quad p = \frac{p'}{\rho g H'} \quad (4)$$

$$u_1 = \frac{u'_1}{\sqrt{gH'}} ; \quad u_2 = \frac{u'_2}{H'/T'} ; \quad \nu_t = \frac{\nu'_t}{H'^2/T'} ; \quad k = \frac{k'}{\sqrt{gH'} H'/T'} \quad (5)$$

$$\sigma = T' \sqrt{\frac{g}{H'}} ; \quad \eta = \frac{\eta'}{H'} ; \quad z_b = \frac{z'_b}{H'} ; \quad h = \frac{h'}{H'} \quad (6)$$

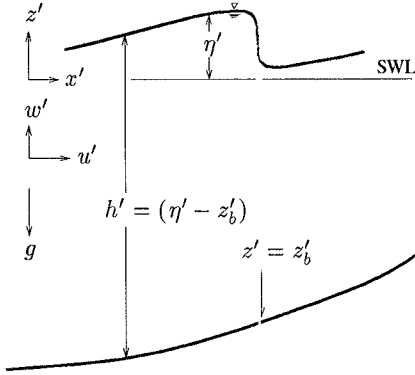


Figure 1: Definition sketch  
 terms of the order of  $\sigma^{-2}$  are neglected in the normalized equations corresponding to (1) and (2).

The conventional notations of  $x = x_1$ ,  $z = x_2$ ,  $u = u_1$  and  $w = u_2$  are used in the following. The simplified depth-integrated continuity and horizontal momentum equations under the assumption of  $\sigma^2 \gg 1$  are expressed as

$$\frac{\partial h}{\partial t} + \frac{\partial q}{\partial x} = 0 \quad (7)$$

$$\frac{\partial q}{\partial t} + \frac{\partial}{\partial x} \left( qU + m + \frac{1}{2}h^2 \right) = -\theta h - \tau_b \quad (8)$$

with

$$m = \int_{z_b}^{\eta} (u - U)^2 dz \quad (9)$$

where  $h$  = water depth given by  $h = (\eta - z_b)$ ;  $q$  = volume flux per unit width;  $U$  = depth-averaged horizontal velocity defined as  $U = q/h$ ;  $\theta$  = normalized bottom slope defined as  $\theta = dz_b/dx$ ;  $\tau_b$  = bottom shear stress; and  $m$  = momentum flux correction due to the vertical variation of the horizontal velocity  $u$ . The vertical momentum equation yields essentially hydrostatic pressure for shallow water.

To include energy dissipation due to wave breaking in Boussinesq equations, Zelt (1991) and Schäffer *et al.* (1992) added a term corresponding to the term for the momentum flux correction  $m$  in (8). Zelt (1991) expressed this additional term in the form of horizontal momentum diffusion with an artificial viscosity. The artificial viscosity was calibrated for breaking solitary waves where the diffusion term was activated using a semi-empirical criterion for solitary wave breaking. On the other hand, Schäffer *et al.* (1992) expressed the additional momentum flux using a simple approach based on a surface roller that represented a passive bulk of water riding on the front of a breaking wave. An empirical geometric method was used to determine the shape and location of the surface rollers during the computation. Unlike the present model, these models do not predict the vertical variations of the fluid velocities.

The equation for the momentum flux correction  $m$  is derived from the depth-integrated instantaneous wave energy equation (Kobayashi and Wurjanto 1992)

$$\frac{\partial E}{\partial t} + \frac{\partial}{\partial x} (E_F) = -D \quad (10)$$

in which  $T'$  and  $H'$  are the reference wave period and height used for the normalization. The parameter  $\sigma$  defined in (6) is the ratio between the horizontal and vertical length scales and is assumed to be much larger than unity.

The normalized variables in (4) and (5) are assumed to be on the order of unity in shallow water. The normalization of  $\nu'_i$  and  $k'$  in (5) is based on the turbulence measurements in a wave flume by Cox *et al.* (1994) which have indicated that  $\nu'_i$  and  $k$  are on the order of unity or less inside and immediately outside the surf zone, respectively. The

The specific energy  $E$  defined as the sum of kinetic and potential energy per unit horizontal area is given by

$$E = \frac{1}{2} (qU + m + \eta^2) \quad \text{for } z_b < 0 \quad (11)$$

$$E = \frac{1}{2} (qU + m + \eta^2 - z_b^2) \quad \text{for } z_b > 0 \quad (12)$$

in which the potential energy is taken to be relative to the potential energy in the absence of wave action with SWL at  $z = 0$ . The energy flux  $E_F$  per unit width is expressed as

$$E_F = \eta q + \frac{1}{2} (qU^2 + 3mU + m_3) \quad (13)$$

with

$$m_3 = \int_{z_b}^{\eta} (u - U)^3 dz \quad (14)$$

in which  $m_3$  = kinetic energy flux correction due to the third moment of the velocity deviation  $(u - U)$  over the depth. The energy dissipation rate  $D$  per unit horizontal area in (10) is given by

$$D = \int_{z_b}^{\eta} \tau \frac{\partial u}{\partial z} dz \quad (15)$$

where use is made of the no slip condition  $u = 0$  at  $z = z_b$ .

The energy dissipation rate  $D$  may be expressed as the sum of dissipation due to bottom friction,  $D_f$ , and dissipation due to wave breaking outside of the wave boundary layer,  $D_B$ . The wave boundary layer is not analyzed explicitly in this numerical model. The energy dissipation rate  $D_f$  inside the wave boundary layer may be estimated by (Jonsson and Carlsen 1976)

$$D_f = \tau_b u_b; \quad \tau_b = f_w |u_b| u_b; \quad f_w = \frac{1}{2} \sigma f'_w \quad (16)$$

where  $u_b$  = near-bottom horizontal velocity immediately outside the wave boundary layer and  $f'_w$  = friction factor (Jonsson 1966). Assuming that the thickness of the wave boundary layer is much smaller than the water depth,  $D_B$  may be estimated as

$$D_B = \int_{z_b}^{\eta} \nu_t \left( \frac{\partial u}{\partial z} \right)^2 dz \quad \text{outside boundary layer} \quad (17)$$

Rearranging the instantaneous wave energy equation (10), the equation for the momentum flux correction  $m$  is derived

$$\frac{\partial m}{\partial t} + \frac{\partial}{\partial x} (3mU + m_3) = 2U \frac{\partial m}{\partial x} - 2(\tau_b \tilde{u}_b + D_B) \quad (18)$$

in which  $\tilde{u}_b = u_b - U$  = near-bottom horizontal velocity correction due to the vertical variation of the horizontal velocity  $u$  outside the wave boundary layer.

In order to express  $m$ ,  $m_3$ , and  $D_B$  in terms of  $\tilde{u}_b$ , the horizontal velocity  $u$  outside the wave boundary layer is assumed to be expressible in the form

$$u(t, x, z) = U(t, x) + \tilde{u}_b(t, x) F(\zeta) \quad (19)$$

with

$$\zeta = [z - z_b(x)]/h(t, x) \quad \text{for } 0 \leq \zeta \leq 1 \quad (20)$$

in which  $F$  = normalized function expressing the vertical variation of the velocity deviation ( $u - U$ ) from  $\zeta = 0$  immediately outside the wave boundary layer to  $\zeta = 1$  at the free surface. Substitution of (19) into the normalized continuity equation corresponding to (1) yields the vertical velocity  $w(t, x, z)$  where  $w = 0$  at  $z = z_b$ . The dimensional turbulent eddy viscosity  $\nu'_t$  outside the wave boundary layer is assumed to be given by

$$\nu'_t = (C_\ell h')^2 \left| \frac{\partial u'}{\partial z'} \right| \quad (21)$$

in which  $C_\ell$  = mixing length parameter. The turbulence measurements inside the surf zone by Cox *et al.* (1994) have indicated that (21) is a reasonable first approximation outside the wave boundary layer and that  $C_\ell$  is on the order of 0.1 ( $C_\ell = 0.1$  is used herein). The corresponding normalized turbulent eddy viscosity  $\nu_t$  defined in (5) is expressed as

$$\nu_t = C_\ell^2 \sigma h^2 \left| \frac{\partial u}{\partial z} \right| \quad (22)$$

Substitution of (19) with (22) into (9), (14), and (17) yields

$$m = C_2 h \tilde{u}_b^2 \quad ; \quad C_2 = \int_0^1 F^2 d\zeta \quad (23)$$

$$m_3 = C_3 h \tilde{u}_b^3 \quad ; \quad C_3 = \int_0^1 F^3 d\zeta \quad (24)$$

$$D_B = C_B C_\ell^2 \sigma |\tilde{u}_b|^3 \quad ; \quad C_B = \int_0^1 \left| \frac{dF}{d\zeta} \right|^3 d\zeta \quad (25)$$

Madsen and Svendsen (1983) and Svendsen and Madsen (1984) assumed a cubic velocity profile for their analyses of a hydraulic jump and a turbulent bore on a beach. Accordingly, the function  $F$  in (23) – (25) outside the wave boundary layer is assumed to be cubic and expressed as

$$F = 1 - (3 + 0.75a)\zeta^2 + a\zeta^3 \quad \text{for } 0 \leq \zeta \leq 1 \quad (26)$$

in which  $a$  = cubic velocity profile parameter. The shear stress  $\tau$  should drop to zero at the free surface. To satisfy  $\frac{\partial u}{\partial z} = 0$  at the free surface,  $a = 4$ . The assumed form (26) results in  $\tau = 0$  at  $\zeta = 0$  immediately outside the wave boundary layer in contradiction with the turbulence measurements inside the surf zone by Cox *et al.* (1994). The cubic profile assumed by Svendsen and Madsen (1984) suggests that the parameter  $a$  is approximately 3 and the range of  $a = 3-4$  is considered in the following. Substitution of (26) into (23) – (25) yields  $C_2$ ,  $C_3$ , and  $C_B$  as a function of  $a$ .

Fig. 2 shows the cubic velocity profile function  $F$  given by (26) as a function of  $\zeta$  for  $a = 3.0, 3.5,$  and  $4.0$ . The abscissa in Fig. 2 is the value of  $-F$  because  $\tilde{u}_b$  is expected to be negative under the wave crest. Fig. 2 hence depicts the normalized vertical variation of the horizontal velocity deviation ( $u - U$ ) under the wave crest. The assumed cubic profile is not sensitive to the parameter  $a$  in the range of  $a = 3-4$  except in the vicinity of the free surface where no velocity data is available inside the surf zone. Fig. 3 shows the parameters  $C_2$ ,  $C_3$  and  $C_B$  as a function of the cubic

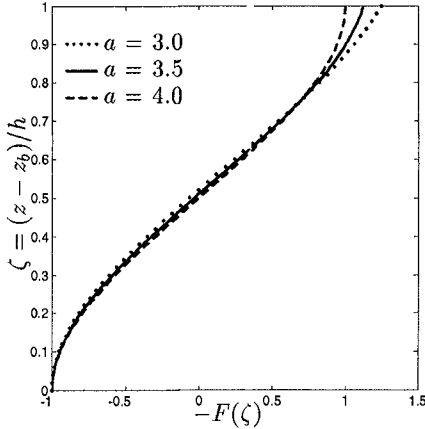


Figure 2: Cubic velocity profile function  $-F$  as a function of  $\zeta$

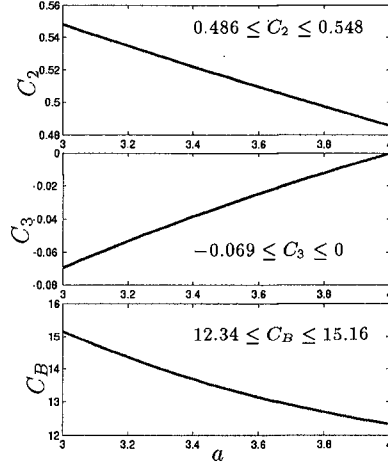


Figure 3:  $C_2$ ,  $C_3$ , and  $C_B$  vs.  $a$

profile parameter  $a$ . These parameters vary little for  $a = 3-4$ . Fig. 3 indicates that  $C_2 \simeq 0.5$ ,  $C_3 \simeq -0.03$  and  $C_B \simeq 13$ . The computed results are also found to be insensitive to  $a$  and in this paper  $a = 3$  for most comparisons with data.

To obtain  $\tilde{u}_b$  for the computed  $h$  and  $m$ , it is assumed that

$$\tilde{u}_b = -\left(\frac{m}{C_2 h}\right)^{1/2} \quad \text{for } U \geq 0 \tag{27}$$

$$\tilde{u}_b = \left(\frac{m}{C_2 h}\right)^{1/2} \quad \text{for } U < 0 \tag{28}$$

which ensures that  $|u_b| \leq |U|$  with  $u_b = (U + \tilde{u}_b)$ .

To examine the degree of numerical dissipation hidden in the computed results, the instantaneous energy equation (10) is averaged over time. The time averaged energy balance is

$$\frac{d}{dx} (\overline{E_F}) = -\overline{D_f} - \overline{D_B} - \overline{D_n} \tag{29}$$

Where the overbar denotes time averaging and  $E_F$ ,  $D_f$ , and  $D_B$  are given by (13), (16), and (25) respectively. The time-averaged numerical dissipation rate  $\overline{D_n}$  is added in (29) so that  $\overline{D_n}$  can be estimated for the computed  $\overline{E_F}$ ,  $\overline{D_f}$ , and  $\overline{D_B}$ .

**Numerical Method**

To solve (7), (8) and (18) for  $h$ ,  $q$ , and  $m$ , these equations are combined in the following vector form:

$$\frac{\partial \mathbf{U}}{\partial t} + \frac{\partial \mathbf{F}}{\partial x} + \mathbf{G} = 0 \tag{30}$$

with

$$\mathbf{U} = \begin{bmatrix} h \\ q \\ m \end{bmatrix} ; \quad \mathbf{F} = \begin{bmatrix} q \\ E_2 \\ E_3 \end{bmatrix} ; \quad \mathbf{G} = \begin{bmatrix} 0 \\ G_2 \\ G_3 \end{bmatrix} \tag{31}$$

and

$$F_2 = qU + m + \frac{1}{2}h^2 \quad ; \quad G_2 = \theta h + \tau_b \quad (32)$$

$$F_3 = 3mU + m_3 \quad ; \quad G_3 = 2 \left( \tau_b \tilde{u}_b + D_B - U \frac{\partial m}{\partial x} \right) \quad (33)$$

Eq. (30) is solved numerically using the MacCormack method (MacCormack 1969) which is a simplified variation of the two-step Lax-Wendroff method (e.g., Anderson *et al.* 1984) and has been applied successfully for the computation of unsteady open channel flows with hydraulic jumps (e.g., Chaudhry 1993). The use of the Lax-Wendroff method for (30) would be very difficult because this method requires the Jacobian of  $\mathbf{F}$  with respect to  $\mathbf{U}$ .

The values of  $\mathbf{U}_j$  at the node  $j$  with  $j = 1, 2, \dots, s$  and at the present time  $t$  are known in the following, where  $s =$  the most landward node. Computation is initiated at time  $t = 0$  with no wave action in the computational domain, thus  $h = q = m = 0$ . The unknown values of  $\mathbf{U}_j^*$  at the node  $j$  and at the next time level  $t^* = (t + \Delta t)$  are denoted by the superscript asterisk. The predictor, corrector and final steps of the MacCormack method are expressed as

$$\dot{\mathbf{U}}_j = \mathbf{U}_j - \frac{\Delta t}{\Delta x} (\mathbf{F}_{j+1} - \mathbf{F}_j) - \Delta t \mathbf{G}_j \quad \text{for } j = 1, 2, \dots, s-1 \quad (34)$$

$$\ddot{\mathbf{U}}_j = \dot{\mathbf{U}}_j - \frac{\Delta t}{\Delta x} (\dot{\mathbf{F}}_j - \dot{\mathbf{F}}_{j-1}) - \Delta t \dot{\mathbf{G}}_j \quad \text{for } j = 2, 3, \dots, s-1 \quad (35)$$

$$\mathbf{U}_j^* = \frac{1}{2} (\mathbf{U}_j + \ddot{\mathbf{U}}_j) \quad \text{for } j = 2, 3, \dots, s-1 \quad (36)$$

The variable time step  $\Delta t$  is calculated by the following approximate expression

$$\Delta t = \frac{C_n \Delta x}{\max(|U_j| + \sqrt{h_j})} \quad \text{for } j = 1, 2, \dots, s \quad (37)$$

in which  $C_n$  is the Courant number and the denominator in (37) is the maximum value of  $(|U_j| + \sqrt{h_j})$  at all the wet nodes.

Use of the MacCormack method results in numerical high-frequency oscillations which tend to appear at the rear of a breaking wave, especially on a gentle slope. For open-channel flows, Chaudhry (1993) summarized a procedure to smooth these high-frequency oscillations. To apply this procedure for breaking waves on slopes excluding the boundary points, the computed water depth  $h_j^*$  at the node  $j$  and at the next time level  $t^*$  is used to calculate the parameter  $\nu_j$  at the node  $j$  defined as

$$\nu_j = \frac{|h_{j+1}^* - 2h_j^* + h_{j-1}^*|}{|h_{j+1}^*| + 2|h_j^*| + |h_{j-1}^*|} \quad \text{for } j = 2, 3, \dots, (s^* - 1) \quad (38)$$

The parameter  $\epsilon_{j+0.5}$  at the midpoint of the nodes  $j$  and  $(j+1)$  is given by

$$\epsilon_{j+0.5} = \kappa \left( \frac{h_j^* + h_{j+1}^*}{2} \right)^{0.5} \max(\nu_j, \nu_{j+1}) \quad \text{for } j = 2, 3, \dots, (s^* - 2) \quad (39)$$

in which  $\kappa$  = numerical damping coefficient for regulating the amount of damping of the high-frequency oscillations. The computed water depth  $h_j^*$  is modified as

$$h_j^* = h_j^* + \epsilon_{j+0.5} (h_{j+1}^* - h_j^*) - \epsilon_{j-0.5} (h_j^* - h_{j-1}^*) \quad \text{for } j = 3, 4, \dots, (s^* - 2) \quad (40)$$

Likewise,  $U_j^*$  and  $m_j^*$  are smoothed using (40) with  $h_j^*$  being replaced by  $U_j^*$  and  $m_j^*$ , respectively, where  $\epsilon_{j+0.5}$  is the same. The smoothed  $h_j^*$  and  $U_j^*$  are used to calculate  $q_j^* = h_j^* U_j^*$ . Chaudhry (1993) suggested expressions of  $\nu_j$  at the boundary points for open-channel flows. However, the addition of these expressions in (39) and (40) is found to produce spurious fluid motions even in the absence of waves on slopes. As a result, the smoothing at the end points is not recommended for breaking waves on slopes. For breaking waves on gentle beach slopes,  $\kappa = 1$  has been used to damp the high-frequency oscillations. For waves surging on steep slopes of coastal structures,  $\kappa = 0.1$  appears to be sufficient. However, the smoothing procedure based on (38) tends to cause more damping near the shoreline where the water depth  $h$  is very small. To remedy this uneven damping, the factor  $[(h_j^* + h_{j+1}^*)/2]^{0.5}$  is included in (39) to reduce the damping near the shoreline.

The landward boundary is located at the moving shoreline on the slope where the water depth is essentially zero and the landward boundary algorithm is a minor extension of the previous one-dimensional algorithm. The seaward boundary conditions on  $h$  and  $q$  utilizes the method of characteristics in basically the same way as the previous models (e.g., Kobayashi and Wurjanto 1989) with the inclusion of the momentum flux correction,  $m$ . However, the value of  $m$  at the seaward boundary needs to be found using (18). The value of  $m$  at  $x = 0$  might be taken as  $m = 0$  at  $x = 0$  if the seaward boundary is located outside the surf zone. This is because the vertical variation of the horizontal velocity assumed in (18) is caused by wave breaking in this numerical model for shallow water waves. However, the boundary condition of  $m = 0$  at  $x = 0$  will yield  $m = 0$  for  $t > 0$  and  $x > 0$  because  $m = 0$  is a trivial solution of (18). It is hence required to introduce  $m \geq 0$  at  $x = 0$  so that  $m \geq 0$  for  $t > 0$  and  $x > 0$ . One option is to rewrite (18) in terms of  $\tilde{u}_b$  as

$$\frac{\partial \tilde{u}_b}{\partial t} + \frac{\partial}{\partial x} (U \tilde{u}_b) = -\frac{C_3 \tilde{u}_b}{2C_2} \left( \frac{\tilde{u}_b}{h} \frac{\partial h}{\partial x} + 3 \frac{\partial \tilde{u}_b}{\partial x} \right) - \frac{\tau_b + C_{B\ell} |\tilde{u}_b| \tilde{u}_b}{C_2 h} \quad (41)$$

where  $C_{B\ell} = C_B C_\ell^2 \sigma$ . Note that  $\tilde{u}_b = 0$  is not a trivial solution of (41). The value of  $m = C_2 h \tilde{u}_b^2$  at  $x = 0$  may then be obtained using the value of  $\tilde{u}_b$  at  $x = 0$  computed using (41) which is approximated by an explicit first-order finite difference.

### Comparison of Previous 1-D and Present Models

To demonstrate the effectiveness of the MacCormack method, the present model VBREAK is reduced to a one-dimensional model and compared with the previous one-dimensional model IBREAK of Kobayashi and Wurjanto (1989). The quasi one-dimensional model uses an explicit first order finite difference of (41) to obtain the value of  $(\tilde{u}_b)_1^*$  and thus  $m_1^*$ , the momentum correction factor at the next time level at the seaward boundary. However, when the value of  $m_1^*$  is set to zero at all times, the computed values of  $m_j^*$  at any node are zero for all times everywhere inside the computational domain. Thus the computed horizontal velocity has no vertical variation through the specification of zero vertical variation at the seaward boundary.

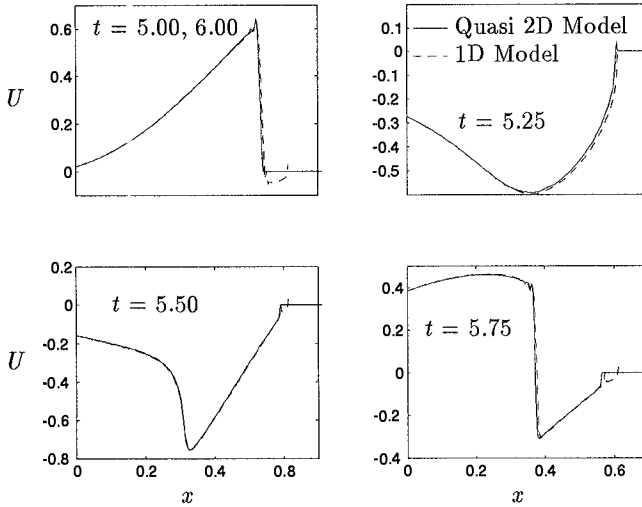


Figure 4: Cross-shore variations of computed depth-averaged velocity  $U$

The only difference, then, between VBREAK and IBREAK is the different numerical methods employed to solve the same governing equations where IBREAK is based on the dissipative Lax-Wendroff method. Use is made of the 1:2.5 riprap revetment test conducted by Ahrens (1975) for the comparison. The computed free surface elevations turn out to be essentially identical while the computed depth-averaged velocities  $U$  display minor differences near the shoreline as shown in Fig. 4. The cross-shore variation of the depth-averaged velocity is depicted at 5 times throughout the final wave period. The computed velocities for each model are identical at  $t = 5$  and 6 due to wave periodicity in Fig. 4.

### Comparison with Data of Stive (1980)

The model is compared with the comprehensive measurements of test 1 presented by Stive (1980) and Stive and Wind (1982). Because the numerical model predicts the vertical variations of the horizontal velocity, the comparison of the measured and computed velocities can be made without any ambiguity. In Stive's test 1, the incident regular waves with period  $T' = 1.79$  s broke as spilling breakers on the 1:40 concrete beach. The seaward boundary for the computation is taken to be at the location of still water depth  $d'_i = 0.2375$  m, where the near-breaking wave profile was shown to be similar to the cnoidal wave profile as explained by Kobayashi *et al.* (1989). The measured wave height at the seaward boundary was  $H' = 0.172$  m. The friction factor of 0.05 is used as in the previous computation by Kobayashi *et al.* (1989). A Courant number of 0.3 is adopted for the stable computation.

The measured and computed temporal variations of the free surface are compared at  $x = 0, 1.29, 2.15,$  and  $3.01$  in Fig. 5. The variation of the free surface from the mean water level  $\bar{\eta}$  for the last wave from  $t = 29.0$  to  $t = 30.0$  is shown in each panel. The crest of the computed wave form has been matched by hand with the measured crest;

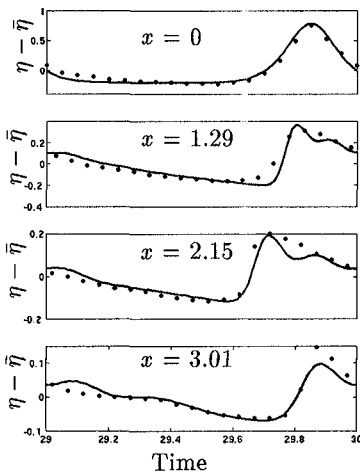


Figure 5: Measured and computed wave profiles.

• Data    - - - Computed  $u$     — Computed  $U$

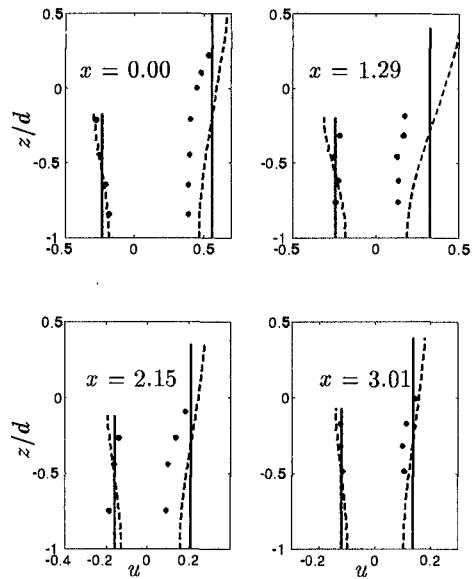


Figure 6: Measured and computed maximum and minimum normalized horizontal velocities

therefore, Fig. 5 should indicate only the comparison of the predicted and measured wave shapes. The first panel shows that the specified incident cnoidal wave at  $x = 0$  agrees well with the measured profile. The high frequency oscillations following the wave crest are apparent in Fig. 5.

The maximum and minimum horizontal velocities at  $x = 0, 1.29, 2.15,$  and  $3.01$  are depicted in Fig. 6. In each panel the dashed line represents the computed horizontal velocity  $u$  and the solid line is the computed depth averaged velocity  $U$ . The vertical axis is the ratio of  $z/d$  where  $z$  is the vertical coordinate and  $d$  is the water depth below SWL. The maximum and minimum values in Fig. 6 are obtained at each elevation  $z$  without regard to the vertical phase differences. Panel one indicates that although the specified and measured free surface elevations match at the seaward boundary well, the maximum horizontal velocity is considerably overpredicted. Likewise, at locations  $x = 1.29, 2.15,$  and  $3.01$  the maximum velocity is overpredicted. The greatest computed variation of the velocity over the depth occurs after breaking, at  $x = 1.29$ . This, however, does not correspond well to the velocity measured below the trough level that displays virtually no variation with depth at  $x = 1.29$ .

### Comparison with Data of Cox *et al.* (1995)

Comparison is also made with the data collected by Cox *et al.* (1995) that included detailed velocity profiles inside the surf zone. The experiment was performed in a wave flume with a 1:35 beach constructed of Plexiglas with a layer of sand glued to the surface to increase the bottom roughness. At each measuring line, water velocity measurements were taken at approximately twenty elevations. The free surface and

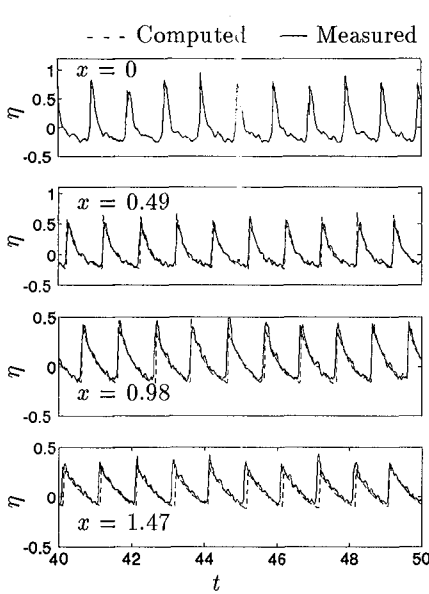


Figure 7: Measured and computed free surface

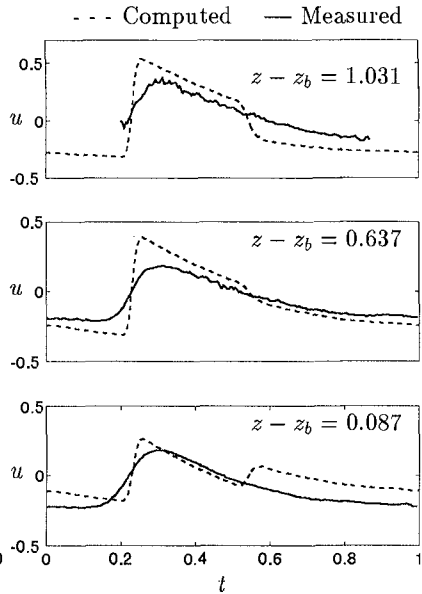


Figure 8: Normalized phase-averaged horizontal velocity  $u$  at three elevations at L4

velocities were measured for the duration of the last 50 waves out of 300 at each line. The numerical model is run with 300 waves of 2.2 s period in order to be consistent with the experimental procedure. The phase averaging is based on the last 50 waves in the same way as the measured data.

The friction factor  $f'_w = 0.05$  is used. A Courant number of 0.4 maintained numerical stability in the following comparison. The seaward boundary is located landward of the break point, at measuring line L3 as defined by Cox *et al.* (1995). The height of the incident regular waves at L3 was  $H' = 12.71$  cm and the corresponding still water depth was 17.71 cm.

Fig. 7 depicts the free surface at  $x = 0.0, 0.49, 0.98,$  and  $1.47$  in the surf zone at L3, L4, L5, and L6 where L denotes the measuring line. The free surface prediction is quite good despite a lagging phase error seen most prominently at  $x = 1.47$ .

Fig. 8 shows the predicted and measured phase-averaged horizontal velocities at three elevations at L4 as a typical example. The first panel shows the velocities near the wave trough level. The solid line represents the measured values excluding dropouts in the data near the free surface. The second panel is a comparison at approximately mid-depth. The near bottom (1.1 cm above the bottom) velocities are plotted in the last panel. The unrealistic kink seen in panels one and three are due to the adopted relations (27) and (28) where the abrupt change in the velocity correction  $\tilde{u}_b$  is assumed to occur with the sign change in the depth averaged velocity,  $U$ .

The measured and computed horizontal and vertical velocity profiles are compared at six equally-spaced phases over one wave period for L5 in Fig. 9. The first panel depicts the computed and measured horizontal velocity as a function of the normalized

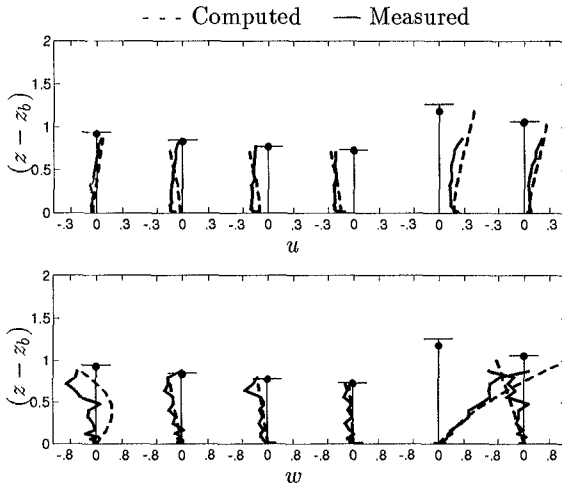


Figure 9: Vertical variations of horizontal and vertical velocities at six phases at L5

vertical distance  $(z - z_b)$  above the bottom. The computed and measured free surfaces are shown as a black dot and as a horizontal line, respectively. The second panel depicts the comparison of the measured and computed vertical velocities at the same six phases. The discrepancy between the measured and computed vertical variations are caused, in part, by the aforementioned phase mismatch. As a whole, the agreement is reasonable in spite of the assumed simple vertical velocity profile (26). This is probably because the comparison is limited to below the wave trough level.

The normalized energy quantities involved in (29) are shown in Fig. 10. The numerical dissipation rate  $\overline{D}_n$  dominates over the dissipation rate due to bottom friction,  $\overline{D}_f$ , and the dissipation rate due to wave breaking,  $\overline{D}_B$ . This clearly indicates the shortcoming of the assumed velocity profile (26) which may be reasonable below the trough level but can not account for the much larger dissipation occurring above the trough level. Velocity data above the trough would be required to improve (26).

## Conclusions

A numerical model is developed to predict the cross-shore and temporal variations of the free surface elevation  $\eta$ , the depth-averaged horizontal velocity  $U$ , and the near-bottom horizontal velocity correction  $\tilde{u}_b$  associated with the momentum flux correction  $m$  due to the vertical variation of the horizontal velocity  $u$  under the action of normally incident breaking waves. The three governing equations required for the three unknown variables are the depth-integrated continuity and horizontal momentum equations together with the new equation for the momentum flux correction  $m$  derived from the depth-integrated wave energy equation.

The normalized vertical profile of the horizontal velocity  $u$  outside the thin wave boundary layer is assumed to be cubic on the basis of limited available data. The turbulent shear stress outside the wave boundary layer is assumed to be expressed using the turbulent eddy viscosity whose mixing length is proportional to the instantaneous water depth. Although two additional empirical parameters are introduced in rela-

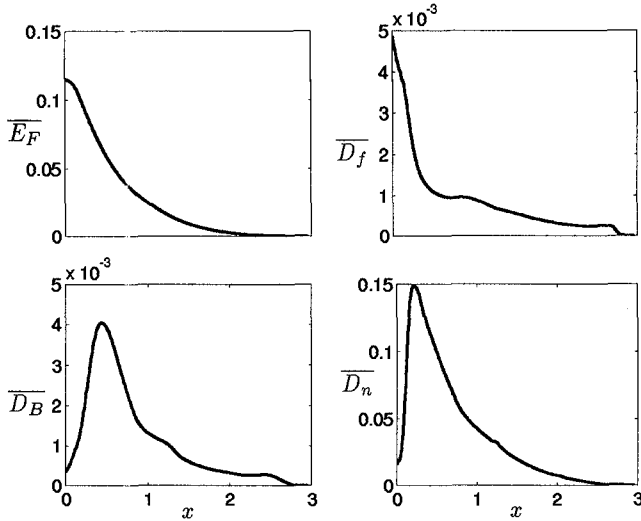


Figure 10: Computed cross-shore variation of normalized energy flux, bottom dissipation, breaking dissipation, and numerical dissipation.

tion to these assumptions, the computed vertical profiles of the horizontal velocity are found to be fairly insensitive to these empirical parameters in their ranges expected from limited available data.

The numerical model is reduced to a one-dimensional model and compared to the previous one-dimensional model. With appropriate simplification of the seaward boundary condition, the momentum flux correction equals zero identically throughout the computation domain for all times. The results are essentially the same for both models. This comparison demonstrates the efficiency and accuracy of the MacCormack method in the solution of the finite-amplitude shallow-water equations. The model is compared with the laboratory data presented by Stive (1980) and Stive and Wind (1982). The free surface elevations are predicted fairly accurately, while the maximum horizontal velocities are consistently overpredicted. The model is compared with the detailed fluid velocity measurements of Cox *et al.* (1995). Again, the free surface elevations are predicted fairly well. The horizontal velocity prediction is satisfactory apart from some phase mismatch and the unrealistic discontinuity in the velocity accompanying the sign change in  $U$ . As a whole, the agreement is reasonable considering the assumed simple vertical velocity profile. However, the model does not offer significant advantages over the previous one-dimensional models.

### Acknowledgments

This work was sponsored by the US Army Research Office, University Research Initiative under contract No. DAAL03-92-G-0116 and by the National Science Foundation under grant No. CTS-9407827.

### References

- Ahrens, J.P., 1975. "Large wave tank tests of riprap stability." *Technical Memo No. 51*, U.S. Army Coastal Engineering Research Center, Ft. Belvoir, VA

- Anderson, D.A., Tannehill, J.C., and Pletcher, R.H., 1984. *Computational fluid mechanics and heat transfer*. Hemisphere, New York, NY.
- Chaudhry, M.H., 1993. *Open-channel flow*. Prentice Hall, Englewood Cliffs, NJ.
- Cox, D.T., Kobayashi, N., and Okayasu, A., 1994. "Vertical variations of fluid velocities and shear stress in surf zones." *Proc. 23rd Coast. Engrg. Conf.*, ASCE, 98-112.
- Cox, D.T., Kobayashi, N., and Okayasu, A., 1995. "Experimental and numerical modeling of surf zone hydrodynamics." *Res. Rept. No. CACR-95-07*, Ctr. for Applied Coast. Res., Univ. of Delaware, Newark, DE.
- Johnson, B.D., Kobayashi, N., and Cox, D.T., 1996. "Formulation and validation of vertically two-dimensional shallow-water wave model." *Res. Rept. No. CACR-96-05*, Ctr. for Applied Coast. Res., Univ. of Delaware, Newark, DE.
- Jonsson, I.G., 1966. "Wave boundary layers and friction factors." *Proc. 10th Coast. Engrg. Conf.*, ASCE, 1, 127-148.
- Jonsson, I.G., and Carlsen, N.A., 1976. "Experimental and theoretical investigations in an oscillatory turbulent boundary layer." *J. Hydraul. Res.*, 14, 45-60.
- Kobayashi, N., DeSilva, G.S., and Watson, K.D., 1989. "Wave transformation and swash oscillation on gentle and steep slopes." *J. Geophys. Res.*, 94(C1), 951-966.
- Kobayashi, N., and Johnson, B.D., 1995. "Numerical model VBREAK for vertically two-dimensional breaking waves on impermeable slopes" *Res. Rept. No. CACR-95-06*, Ctr. for Applied Coast. Res., Univ. of Delaware, Newark, DE.
- Kobayashi, N., and Wurjanto, A., 1989. "Numerical model for design of impermeable coastal structures." *Res. Rept. No. CE-89-75*, Ctr. for Applied Coast. Res., Univ. of Delaware, Newark, DE.
- Kobayashi, N., and Wurjanto, A., 1992. "Irregular wave setup and run-up on beaches." *J. Wtrwy. Port, Coast. and Oc. Engrg.*, ASCE, 118(4), 368-386.
- MacCormack, R.W., 1969. "The effect of viscosity in hypervelocity impact cratering." *Paper 69-354*, Am. Inst. of Aeronaut. and Astronaut., New York.
- Madsen, P.A., and Svendsen, I.A., 1983. "Turbulent bores and hydraulic jumps." *J. Fluid Mech.*, 129, 1-25.
- Rodi, W., 1980. *Turbulence models and their application in hydraulics*. Intl. Assoc. Hydraul. Res., Delft, the Netherlands.
- Schäffer, H.A., Deigaard, R., and Madsen, P., 1992. "A two-dimensional surf zone model based on the Boussinesq equations." *Proc. 23rd Coast. Engrg. Conf.*, ASCE, 1, 576-589
- Stive, M.J.F., 1980. "Velocity and pressure field of spilling breakers." *Proc. 17th Coast. Engrg. Conf.*, ASCE, 547-566.
- Stive, M.J.F., and Wind, H.G., 1982. "A study of radiation stress and set-up in the nearshore region." *J. Coast. Engrg.*, 6, 1-25.
- Svendsen, I.A., and Madsen, P.A., 1984. "A turbulent bore on a beach." *J. Fluid Mech.*, 148, 73-96.
- Zelt, J.A., 1991. "The run-up of nonbreaking and breaking solitary waves." *J. Coast. Engrg.*, 15, 205-246.